Regulation of Thalamocortical Patterning and Synaptic Maturation by NeuroD2

Gulayse Ince-Dunn,[1,6] Benjamin J. Hall,[1,2,6]
Shu-Ching Hu,[1,5] Beth Ripley,[2] Richard L. Huganir,[1,4]
James M. Olson,[3] Stephen J. Tapscott,[3]
and Anirvan Ghosh[1,2,*]

[1] Department of Neuroscience
Johns Hopkins University School of Medicine
Baltimore, Maryland 21205
[2] Neurobiology Section
Division of Biological Sciences
University of California, San Diego
La Jolla, California 92093
[3] Clinical Research and Human Biology Divisions and
 Program in Developmental Biology
Fred Hutchinson Cancer Research Center
Seattle, Washington 98109
[4] Howard Hughes Medical Institute
Johns Hopkins University School of Medicine
Baltimore, Maryland 21205

Summary

During cortical development, both activity-dependent and genetically determined mechanisms are required to establish proper neuronal connectivity. While activity-dependent transcription may link the two processes, specific transcription factors that mediate such a process have not been identified. We identified the basic helix-loop-helix (bHLH) transcription factor Neurogenic Differentiation 2 (NeuroD2) in a screen for calcium-regulated transcription factors and report that it is required for the proper development of thalamocortical connections. In *neuroD2* null mice, thalamocortical axon terminals fail to segregate in the somatosensory cortex, and the postsynaptic barrel organization is disrupted. Additionally, synaptic transmission is defective at thalamocortical synapses in *neuroD2* null mice. Total excitatory synaptic currents are reduced in layer IV in the knockouts, and the relative contribution of AMPA and NMDA receptor-mediated currents to evoked responses is decreased. These observations indicate that NeuroD2 plays a critical role in regulating synaptic maturation and the patterning of thalamocortical connections.

Introduction

Much of our understanding of the development of neuronal connections and maps in the neocortex comes from studies investigating the formation of sensory systems. In the rodent somatosensory system, tactile input from whiskers is conveyed to the cortex via the brainstem and thalamus. Clusters of axon terminals in the brainstem, thalamus, and layer IV cortex form an orderly array of anatomical and functional units representing a topographic map of the whisker field and are called the barrelettes, barreloids, and barrels, respectively (Woolsey and Van der Loos, 1970; Wallace, 1987; Welker, 1976).

The development of proper connections from the periphery to subcortical relay stations and eventually to the cortex requires neuronal activity (reviewed in Katz and Shatz, 1996; Crair, 1999; Erzurumlu and Kind, 2001; Fox, 2002). Genetic manipulations that disrupt synaptic activity result in failure of barrel formation in layer IV. For example, a cortex-specific knockout of the NR1 subunit of the NMDA receptor results in diffuse clustering of the thalamocortical axon (TCA) terminals in the cortex and a complete inability of cortical neurons to form barrel-related structures in layer IV (Iwasato et al., 2000; S. Konur and A.G., unpublished data). Similarly, mice that lack the mGluR5 subunit of the metabotropic glutamate receptors fail to cluster their TCA terminals into barrel domains in the cortex (Hannan et al., 2001).

The segregation of thalamocortical axons is accompanied by changes in synaptic function in barrel cortex. Initially, thalamocortical synaptic currents are mediated mainly by NMDA receptors, with little AMPA receptor contribution. However, after the first postnatal week the NMDA receptor contribution decreases and the AMPA currents increase (Lu et al., 2001). The switch in the relative contributions of NMDA and AMPA receptor-mediated currents coincides with a loss of ability to induce long-term potentiation (LTP) and long-term depression (LTD) at this synapse (Crair and Malenka, 1995; Isaac et al., 1997; Lu et al., 2001; Feldman et al., 1998). The mouse adenylyl cyclase 1 (AC1) mutant, which lacks barrel organization of TCAs, has a reduced contribution of AMPA receptor-mediated currents, suggesting a link between the development of AMPA currents and the maturation of barrel cortex (Abdel-Majid et al., 1998; Lu et al., 2003).

While synaptic transmission appears to play an important role in the development of thalamocortical connections, the mechanisms downstream of receptor activation that regulate thalamocortical patterning are only now beginning to be explored. The involvement of NMDA receptors in the development of both visual and barrel cortex, and the involvement of metabotropic glutamate receptors in barrel cortex development, suggests that calcium signaling is likely to play an important role. Calcium influx can influence synaptic function both by rapid modification of synaptic proteins as well as by regulating calcium-dependent transcription (reviewed in Ghosh and Greenberg, 1995; West et al., 2001). Consistent with a potential role for calcium-dependent transcription in thalamocortical patterning, it has been shown that sensory stimulation can induce gene expression in the developing cortex (Rosen et al., 1992; Pham et al., 1999; Lein and Shatz, 2000).

To identify transcription factors that might contribute to activity-dependent development in the cortex, we developed a strategy called "transactivator trap" to clone calcium-activated transcription factors in cortical

neurons (Aizawa et al., 2004). This screen led to the identification of several genes not previously known to be involved in activity-dependent development. The first of these genes, *crest*, plays an important role in calcium-dependent dendritic growth (Aizawa et al., 2004). Here we describe our analysis of *neuroD2*, the second gene cloned in the screen. We report that NeuroD2 plays a critical role in the patterning of barrel cortex during development and regulates the maturation of excitatory synapses in the cortex.

Results

Transcriptional Activation by NeuroD2

The transactivator trap screen used to clone NeuroD2 has been previously described (Aizawa et al., 2004). The screen relies on the ability of a Gal4DBD (Gal4 DNA binding domain) fusion protein to mediate calcium-dependent transcription of a UAS-CAT reporter vector. The original *neuroD2* clone that we isolated from the screen contained amino acids 248–383 (the carboxyl terminus) of NeuroD2. We examined the ability of Gal4DBD-NeuroD2 (248-383) to mediate depolarization-induced transactivation in E18 cortical neurons that were transfected with Gal4DBD-NeuroD2 and UAS-CAT at 3 days in vitro (DIV) and stimulated with 50 mM KCl at 4DIV. As a positive control we used a Gal4DBD fusion of CREB, which is known to mediate calcium-dependent transcription. Reporter activity was detected by immunocytochemistry for chloramphenicol acetyl transferase (CAT) protein. Whereas there were few CAT-positive neurons in unstimulated plates, there was a marked increase in CAT-positive neurons following stimulation in Gal4DBD-NeuroD2 and Gal4DBD-CREB-transfected neurons (Figure 1A–1F). This was not seen in neurons transfected with UAS-CAT and the parent vector expressing the Gal4DBD alone. These results indicate that the C terminus of NeuroD2 can mediate depolarization-induced transactivation.

To identify the domains of NeuroD2 that are required for depolarization-induced transactivation, we tested Gal4DBD fusions of full-length NeuroD2 as well as a series of deletion constructs. Only the deletion fragments containing amino acids 294–383 and 248–383 were effective in mediating depolarization-induced transactivation, suggesting that the carboxy terminus of NeuroD2 contains a depolarization-sensitive activation domain (Figures 1G and 1H). The 248–383 fragment consistently had higher basal transactivation compared to the 294–383 fragment, suggesting the presence of an inhibitory domain between amino acids 248 and 294. The fact that full-length Gal4 fusion of NeuroD2 does not mediate activity-dependent transactivation is surprising, since it contains the activation domain. One possibility is that homodimerization induced by Gal4DBD is not compatible with transactivation by the full-length protein since bHLH proteins normally are in a heterodimeric complex with E proteins (E12/E47). Alternatively, NeuroD2 might need to directly bind DNA through its basic domain as opposed to Gal4DBD domain for maximal transcriptional activity.

To assess the ability of full-length NeuroD2 to mediate depolarization-induced transactivation, we examined

activation of the GAP-43 promoter, since it contains multiple E box (CANNTG) elements and NeuroD2 has been reported to bind this promoter (McCormick et al., 1996). As shown in Figure 1I, membrane depolarization leads to activation of the GAP-43-luciferase reporter when transfected into E18 cortical neurons. Transfection of full-length NeuroD2 (1–383) significantly enhances depolarization-induced activation of the reporter. This enhancement is not seen in cultures transfected with a NeuroD2 fragment (1–210) that lacks the C terminus of NeuroD2. These experiments suggest that NeuroD2 can mediate depolarization-dependent activation of the GAP-43 promoter by a mechanism that requires its C terminus domain.

To determine if depolarization-induced activation of NeuroD2 was calcium dependent, we examined the effects of chelating calcium on NeuroD2-dependent activation of the GAP-43-luciferase reporter. As shown in Figure 1J, depolarization and NeuroD2-dependent activation of the GAP-43-luciferase reporter was suppressed by the calcium chelator EGTA. Activation of the reporter by depolarization was also suppressed by the L-type voltage-sensitive calcium channel (L-VSCC) blocker nimodipine. Therefore, depolarization-induced activation of NeuroD2-mediated transcription is calcium dependent.

While our observations suggest that calcium influx activates NeuroD2-mediated transcription, it is possible that the effects we observe on reporter activity are a result of increased NeuroD2 expression as opposed to increased NeuroD2 activation. To determine whether induction of the GAP-43-luciferase reporter was due to an increase in calcium-dependent expression or activation of NeuroD2, we subcloned neuroD2 into two different expression plasmids (pRK5 and pBOS) and asked whether increased expression of NeuroD2 was sufficient to drive reporter activity. Although NeuroD2-*myc* expression was dramatically higher from the pBOS (EF-1 promoter) vector compared to the pRK5 (CMV promoter) vector, it did not lead to increased levels of reporter activity. Thus, increased expression of NeuroD2 does not account for increased reporter activity (see Figure S1 in the Supplemental Data available online). Instead, the marked increase in reporter activity seen following depolarization reflects calcium-dependent activation of NeuroD2-mediated transcription.

NeuroD2 Expression in the Developing Cortex

The ability of NeuroD2 to mediate calcium-dependent transactivation as well as the ability of NeuroD2 to induce GAP-43 expression motivated us to investigate the role of NeuroD2 in development of connections in the cortex. We examined the pattern of *neuroD2* expression in the postnatal brain by taking advantage of a mouse line in which the entire *neuroD2* coding region was replaced with the β-galactosidase gene (Olson et al., 2001; Lin et al., 2004). Staining for β-galactosidase in *neuroD2* (lacZ/+) mice allows one to determine the expression pattern of *neuroD2* in various tissues. We focused our analysis on the cortex during the first postnatal week, since this is the period during which thalamic axons segregate into barrel-specific patterns. On the day of birth, *neuroD2* was expressed weakly but uniformly in layers V and VI of the neocortex (Figures 2A
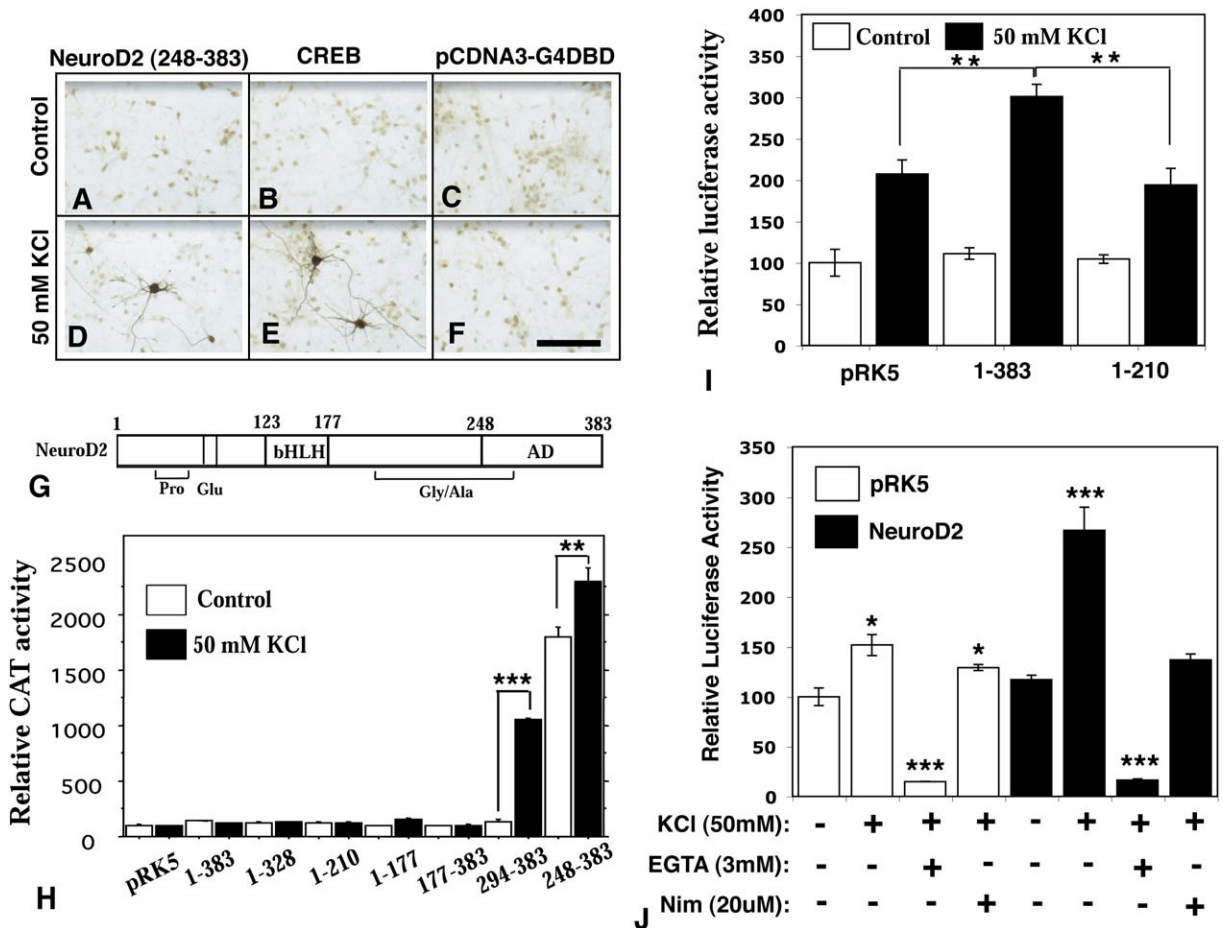
Figure 1. Identification of *neuroD2* Using Transactivator Trap

(A–F) E18 cortical neurons were transfected with Gal4DBD-NeuroD2, Gal4DBD-CREB, or pCDNA3-Gal4DBD together with UAS-CAT at 3DIV, stimulated with 50 mM KCl the next day, and fixed 16 hr later for anti-CAT immunohistochemistry.

(G) Schematic representation of the protein domains of full-length NeuroD2.

(H) Gal4DBD-NeuroD2 fusion constructs and UAS-CAT reporter were transfected and stimulated as described above. After stimulation, cells were harvested for CAT assay. Relative CAT activity is plotted for each NeuroD2 fragment in control and stimulated conditions.

(I) Neurons were cotransfected with full-length NeuroD2 (1-383) or NeuroD2 (1-210) together with GAP-43-luciferase, stimulated with 50 mM KCl at 4DIV, and analyzed for luciferase activity at 5DIV.

(J) Neurons were cotransfected with NeuroD2 (1-383) and GAP-43-luciferase at 3DIV, stimulated with KCl, in the absence or presence of drugs as indicated (3 mM EGTA or 20 μM nimodipine) at 4DIV, and analyzed for luciferase activity at 5DIV. Drugs were bath applied to cultures 1 hr prior to and during KCl stimulation.

For all the transcription assays, SV40-Renilla luciferase construct was cotransfected with the plasmids of interest as an internal transfection control. All CAT and luciferase measurements were normalized to SV40-Renilla luciferase signals. Data in (H)–(J) represent averages from three independent experiments and are presented as mean $\pm$ SD. *p < 0.05, **p < 0.01, ***p < 0.005 by t test. Scale bar, 200 μm.

and 2B). By postnatal day 4 (P4), *neuroD2* expression was detected in all layers of the neocortex, and by P7 it was highly expressed in layer IV neurons as well as in layers II/III, V, and VI (Figures 2C–2F). At P7 we detected strong expression in layer IV, particularly in the barrel cortex (boxed area in Figure 2E). The laminar specificity of *neuroD2* expression was less pronounced in the other areas of the cortex. We did not observe expression of NeuroD2 in any of the thalamic nuclei at the ages we analyzed. The spatiotemporal expression pattern of *neuroD2* correlated well with the period of segregation of thalamic axons in barrel cortex and the maturation of thalamocortical synapses. These observations suggested that NeuroD2 might play an important role in the development of thalamocortical connections in barrel cortex.

Absence of Cortical Barrels in *neuroD2* Null Mice

Cortical barrels emerge during the first postnatal week as thalamic axons segregate into whisker-specific domains in layer IV. A commonly used technique to visualize barrels is to stain for cytochrome oxidase (CO) enzyme activity, which is a mitochondrial enzyme present at high levels in both TCA terminals and in postsynaptic dendrites (Welker, 1976). Comparison of CO staining in wild-type and *neuroD2* null mice revealed that the organization of the barrel field was completely disrupted in *neuroD2* null mice (Figures 3A–3D). While the barrel structures were clearly visible in both the wild-type and heterozygote mice, we observed only diffuse staining in coronal and tangential sections through the barrel cortex of *neuroD2* null mice at P7 and P14 (n = 7) (Figures 3A–3D and Figure S2). The spatial
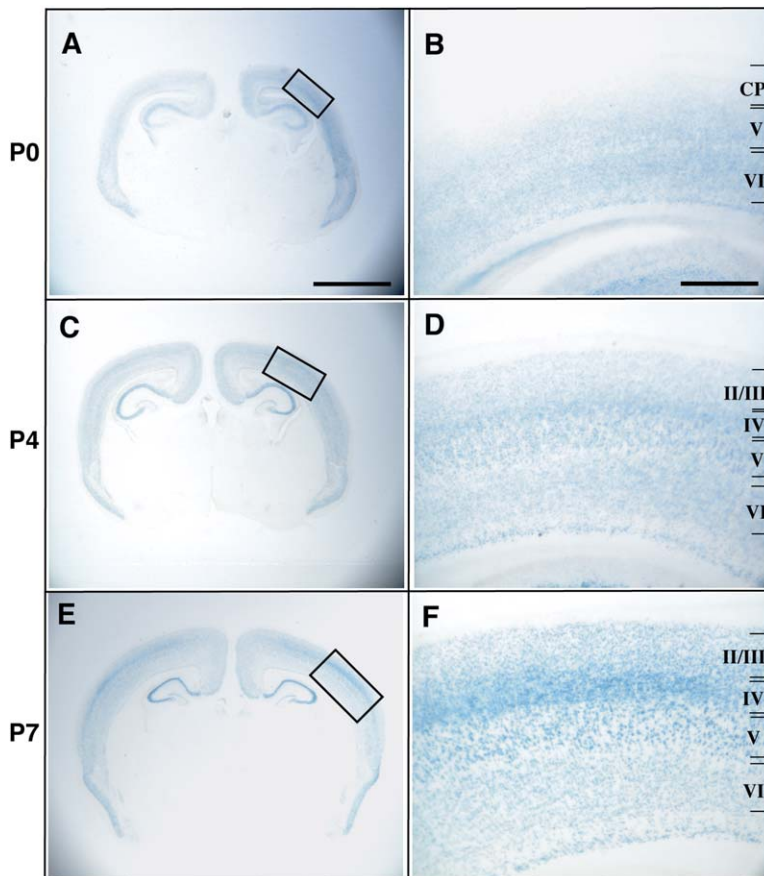
Figure 2. Expression Pattern of *neuroD2* in Early Postnatal Mouse Brain

Heterozygote *neuroD2* mice (lacZ/+) were perfused at the indicated ages, sectioned in the coronal plane, and stained for β-galactosidase activity. Images were captured using brightfield microscopy. (B), (D), and (F) are high-magnification images of regions boxed in (A), (C), and (E). Layers II/III through VI are indicated. CP, cortical plate. Scale bars, 2 mm (A, C, and E) and 0.3 mm (B, D, and F).

organization of layer IV neurons in barrel cortex can be clearly visualized using the nuclear dye Hoechst 33258. Consistent with the CO staining data, in control mice we were able to detect the organization of cortical neurons into barrel structures with cell-sparse domains inside the barrels and cell-dense areas in the septal regions (Figure 3E). The *neuroD2* null mice displayed a diffuse Hoechst staining pattern through layer IV and an overall absence of barrel patterns (Figure 3F). The disruption was not a transient phenomenon, since the barrels were disrupted in *neuroD2* nulls also at P21 (data not shown). These results indicate that NeuroD2 function is required for the proper segregation of barrels in somatosensory cortex.

To determine if the generation of neurons and glial cells was affected in *neuroD2* mutant mice, we examined the distribution of a neuronal (NeuN) and astrocytic (S100-β) antigen by immunofluorescence (Figures 3G–3J) in P7 coronal sections. While the overall pattern of NeuN immunofluoresence was similar in the three genotypes, the border between layers was less pronounced in *neuroD2* nulls compared to wild-type mice (Figures 3G and 3H). We did not detect any difference in the distribution of astrocytes in the neocortex based on S100-β immunofluorescence (Figures 3I and 3J).

We also examined the overall organization of the brain and cell survival in wild-type, heterozygote, and *neuroD2* null mice (Figure S2). The brains of *neuroD2* heterozygotes and knockouts were slightly smaller than that of wild-type littermates, and the hippocampus was smaller and more round in the CA3 area. The corpus callosum failed to form in *neuroD2* heterozygote and null mice, which is a feature seen in several lines of knockout mice (Shen et al., 2002; Qiu et al., 1996). These morphological effects do not account for the barrel cortex defect seen in *neuroD2* null mice, since barrels are clearly visible in *neuroD2* heterozygous mice, although their brains share the same morphology seen in the *neuroD2* nulls.

To determine if there was increased cell death in the cortex in *neuroD2* null mice, which could contribute to the defects in barrel cortex, we quantified apoptotic nuclei in *neuroD2* mutant and control brain sections after TUNEL staining. There was no difference in the number of TUNEL-positive neurons in the three genotypes, indicating that loss of *neuroD2* does not affect cell survival in the developing cortex (Figure S3).

Failure of Thalamocortical Axon Segregation in *neuroD2* Null Mice

To determine if the patterning defect in the barrel cortex of neuroD2 null mice reflected a failure of thalamocortical axon segregation, we labeled thalamic axon terminals using the lipophilic tracer DiI. We injected DiI crystals into the thalamus of wild-type and *neuroD2* knockout mice at P7 and visualized transported label in thalamic afferents by confocal fluorescence microscopy. In control animals, the DiI-labeled TCA terminals were clearly seen in the barrel centers and were excluded from the septal regions (Figure 4A). In contrast,
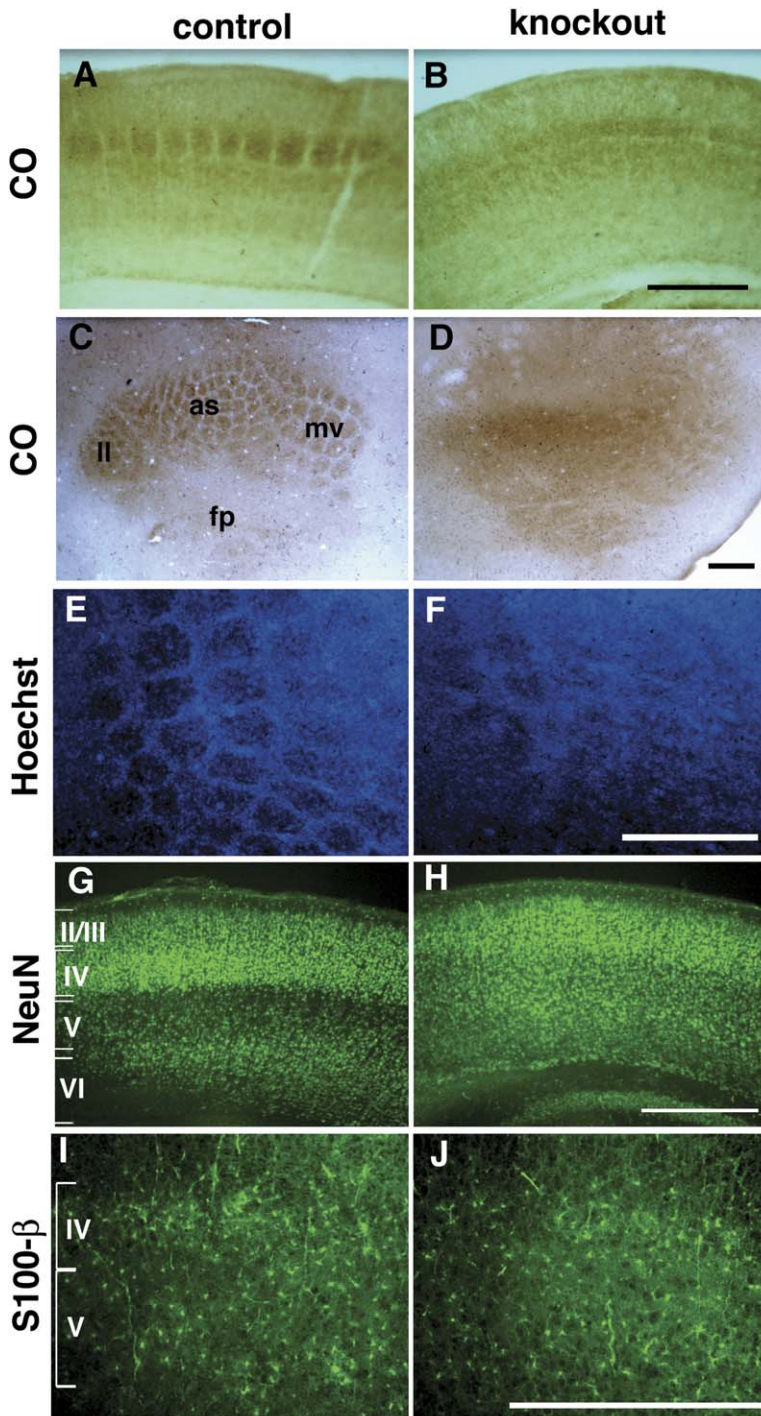
Figure 3. Development of Cortical Barrels Is Disrupted in the *neuroD2* Null Mice

(A–D) Control and *neuroD2* null cortical sections were stained with cytochrome oxidase (CO) to visualize the barrel field. Coronal sections through barrel cortex (A and B) and tangential sections through layer IV (C and D) reveal that the organization of barrels in *neuroD2* null mice is completely disrupted. (E and F) Hoechst 33258 staining of cortical cell bodies display defective organization in knockout mice. (G–J) Distribution of neurons and astrocytes were imaged by immunofluoresence using specific antibodies against NeuN (G and H) and S100-β (I and J) proteins. ll, lower lip; as, anterior snout; fp, forepaw; mv, mystachial vibrissae. Data shown are representative examples based on analysis of seven wild-type/knockout pairs for CO staining and two pairs for Hoechst, NeuN, and S-100β staining. Scale bars, 500 μm.

TCA terminals in the barrel cortex of *neuroD2* null mice were poorly organized. Even though their TCA terminals were localized to layer IV, they did not display fine segregation into barrel structures, indicating a failure in the refinement of the thalamocortical projection (Figure 4B).

An alternate way to visualize thalamocortical afferents without staining neuronal somas or dendrites is to use serotonin (5-HT) immunohistochemistry. This is because during the first 10 days of postnatal life the 5-HT transporter SERT is present in the TCA terminals and imports 5-HT into the terminals (Lebrand et al., 1996). 5-HT immunocytochemistry in coronal as well as tangential sections of P7 mice revealed clear segregation of thalamic axons in control mice but failure of barrel patterning in *neuroD2* null mice, supporting the conclusion that NeuroD2 function is required for the proper segregation of thalamic afferents in barrel cortex (Figure S4).

To determine if the topographical organization of thalamic projections to the cortex was also disrupted in *neuroD2* null mice, we retrogradely labeled thalamic neurons from the cortex using two different lipophilic dyes: DiI and DiA. We placed DiI and DiA crystals at
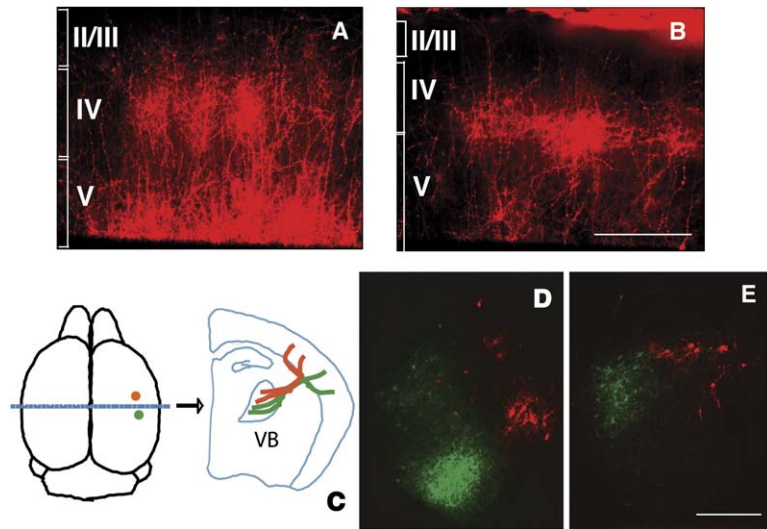
Figure 4. Thalamocortical Axons of *neuroD2* Null Mice Fail to Segregate in Layer IV of Cortex but Are Topographically Organized

(A and B) DiI crystals were injected into the thalamus of paraformaldehyde-fixed control and *neuroD2* knockout littermates at P7. After 4 weeks, the organization of TCA in barrels in coronal sections was visualized by confocal fluorescence microscopy. TCAs were clearly organized into barrels in control mice (A), but the segregation of axons was disrupted in *neuroD2* null mice (B).

(C–E) DiI (red) and DiA (green) crystals were placed in two distinct points within the somatosensory cortex (C). After 5 weeks, brains were sectioned and thalamic cell bodies were visualized (D and E). Retrogradely transported DiI- and DiA-labeled nonoverlapping populations of thalamic neurons in the VB nucleus of the thalamus in control (D) and *neuroD2* null mice (E).

Data shown are representative examples based on analysis of three wild-type/knockout pairs. Scale bars, 200 μm.

two distinct points within the barrel cortex of paraformaldehyde-fixed mice at P0 and after several weeks visualized the retrogradely transported dye in thalamic cell bodies (Figure 4C). At this age, the thalamic axons have grown into layer IV (Agmon et al., 1993; Senft and Woolsey, 1991). The relative position of retrogradely labeled cells in ventrobasal (VB) nucleus was comparable in wild-type and *neuroD2* null mice, suggesting that the overall topography of TCA projections does not require NeuroD2 function (Figures 4D and 4E). These observations indicate that the axons from the VB nucleus of the thalamus are able to project in the correct topography to their final destinations in the barrel cortex, but they are unable to segregate into distinct barrel domains within layer IV in the absence of NeuroD2.

It is possible that the failure to form cortical barrels in the cortex of *neuroD2* null mice is secondary to an earlier disruption in a subcortical relay structure. To examine this possibility, we visualized thalamic barreloids in the VB nucleus and brainstem barelletes in the nucleus principalis of the trigeminal complex by CO staining. The brainstem barrellettes were normal in all the knockouts we visualized (Figures 5E and 5F). The thalamic barreloids of the knockouts were clearly identifiable, although the borders were somewhat less pronounced compared to controls (Figures 5C and 5D). However, in every littermate pair we analyzed, the cortical barrel structures were completely absent or barely visible (Figures 5A and 5B). Thus, the principal defect in the somatosensory system in NeuroD2 null mice appears to be in the cortex, which is consistent with the pattern of NeuroD2 expression.

Synaptic Defects in *neuroD2* Null Mice

The segregation of thalamic axons into barrels is accompanied by functional maturation of the thalamocortical synapse. Since the refinement of thalamic axon terminals is an activity-dependent event, we were interested in determining whether NeuroD2 function was required for the development of synaptic connections in layer IV. We recorded whole-cell currents from
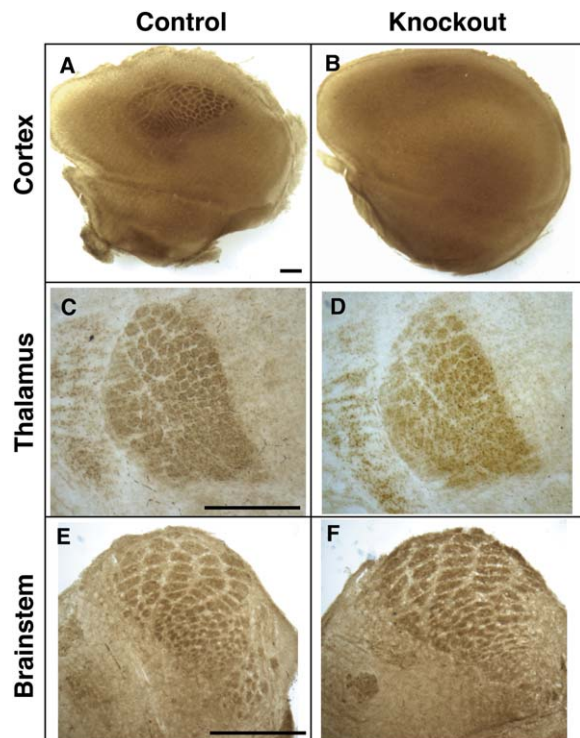
Figure 5. Subcortical Organization of the Somatosensory System in the *neuroD2* Null Mice

(A and B) Tangential sections were cut through layer IV of cortex in control (A) and *neuroD2* null (B) brains and processed for CO staining. Although the whole hemisphere was sectioned tangentially, barrel patterns were not detected in any of the sections in the *neuroD2* null brains.

(C–F) Coronal sections were cut through thalamus (C and D) and brainstem (E and F) and processed for CO staining. Barreloid and barrellette organization was similar in the wild-type and knockout samples.

Data shown are representative examples based on analysis of seven wild-type/knockout pairs. Scale bars, 500 μm.
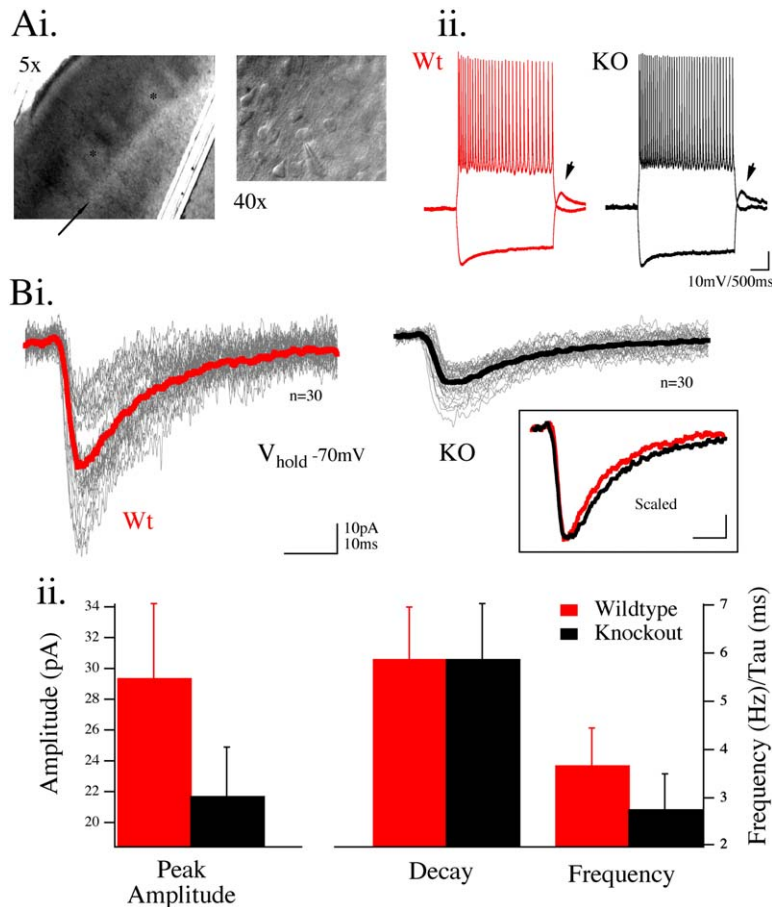
Figure 6. Electrophysiological Properties of Layer IV Neurons in Wild-Type and *neuroD2* Null Mice

(Ai) Barrel columns in layer IV are apparent at 5× magnification in a wild-type cortical slice. Asterisks mark barrel centers, which were used to target placement of recording electrodes. The less dense region below barrel columns (layer 5A, arrow) was used to determine the relative position for recordings in knockout animals. An IR-DIC image at 40× shows the typical pyramidal morphology and characteristic apical dendrite of the recorded neurons.

(Aii) Intrinsic responses to current injection in current-clamp mode were similar between knockout and wild-type cells tested (n = 3). These example responses exhibited strong after-hyperpolarization rebound (arrows) characteristic of all neurons examined, and a spike train in response to depolarizing current typical of regular spiking cortical neurons. Current injection was 50 pA depolarizing and −70 pA hyperpolarizing.

(Bi) Spontaneous synaptic currents observed under voltage clamp in KO slices provide evidence of proper targeting and innervation of these neurons; however, the peak amplitude of spontaneous EPSCs recorded at –70 mV was suppressed. Example traces of spontaneous EPSCs from two littermate animals (30 traces each) are shown with overlaid averages. Current kinetics in both genetic conditions are nearly identical as shown by the scaled overlay (inset).

(Bii) Cumulative data (n = 7 cells; 490 KO events and 995 wt events) confirm that both decay and frequency of events is unchanged but the peak amplitude of spontaneous currents recorded at –70 mV is reduced.

Data are shown as mean ± SD.

layer IV pyramidal neurons in acutely dissected slices from P11/P12 animals. Barrels were visualized in coronal slices using IR-DIC illumination (Figure 6Ai). The lower limit of barrels in layer IV was bounded by a layer of relatively low cell density (layer Va) and was used as a landmark for recordings. We examined the intrinsic properties of layer IV neurons using current-clamp configuration and a potassium gluconate-based recording solution. Neurons within barrels could be classified as either intrinsically bursting or regular spiking based upon their action potential firing properties, and all recorded neurons exhibited strong post-hyperpolarization rebound. Therefore, with respect to basic intrinsic properties, *neuroD2* null layer IV neurons were similar to controls (Figure 6Aii, n = 3). The I/V relationship in both knockout and control neurons was ohmic around resting membrane potential.

To determine if synaptic responses were affected in *neuroD2* null mice, we used voltage-clamp recordings to analyze spontaneous synaptic events from seven cells from each genotype at a holding potential of –70 mV (total of 995 events in wt and 490 events in KO). While total current was decreased in *neuroD2* null slices, both the frequency and decay kinetics of the responses were unchanged, suggesting that the decrease in spontaneous EPSCs was likely to be due to a postsynaptic defect (Figure 6B).

To determine if loss of NeuroD2 led to a defect in evoked postsynaptic responses, we recorded responses in layer IV pyramidal neurons following bipolar stimulation of white matter in acute thalamocortical slices (Agmon and Connors, 1992) (Figure 7A). Brief (100–500 μs) stimulation resulted in evoked responses in layer IV neurons (V_{hold} –70 mV) in both wild-type and *neuroD2* null slices that were completely abolished by CNQX or DNQX (25 μM) and exhibited strong depression in response to paired stimulation (mean 29% at 2 s) (data not shown).

The relative contribution of different subtypes of ionotropic glutamate receptors (iGluRs) is dynamically regulated at thalamocortical synapses during development. Immature synapses are dominated by NMDA receptor-mediated currents. Gradually there is increased expression and insertion of AMPA receptors at synapses, which carries most of the synaptic current in adults. To dissect the relative contribution of the ionotropic glutamate receptors to the postsynaptic response in wild-type and neuroD2 null mice, we recorded evoked synaptic currents at different holding potentials in the presence of a $GABA_A$ antagonist (gabazine, 10 μM) to isolate glutamate receptor currents and a low concentration of DNQX (0.2 μM) to avoid overexcitation and epileptiform activity (Lu et al., 2001). Synaptic currents evoked at –70 mV are primarily AMPA and kainate (KA) mediated,

A

Heterozygote   Knockout

B

$10\mu M$ GABAZINE / $0.2\mu M$ DNQX

Het.   KO

+70   +70

-70   -70

ratio - 0.50   ratio - 0.10

25pA/50ms

C Ratios -70mV/+70mV

n=6

*

n=6

Het./Wt.   KO

D $10\mu M$ Gabazine/ $0.2\mu M$ DNQX
$100\mu M$ dl-APV

Het.

KO

25pA
3ms
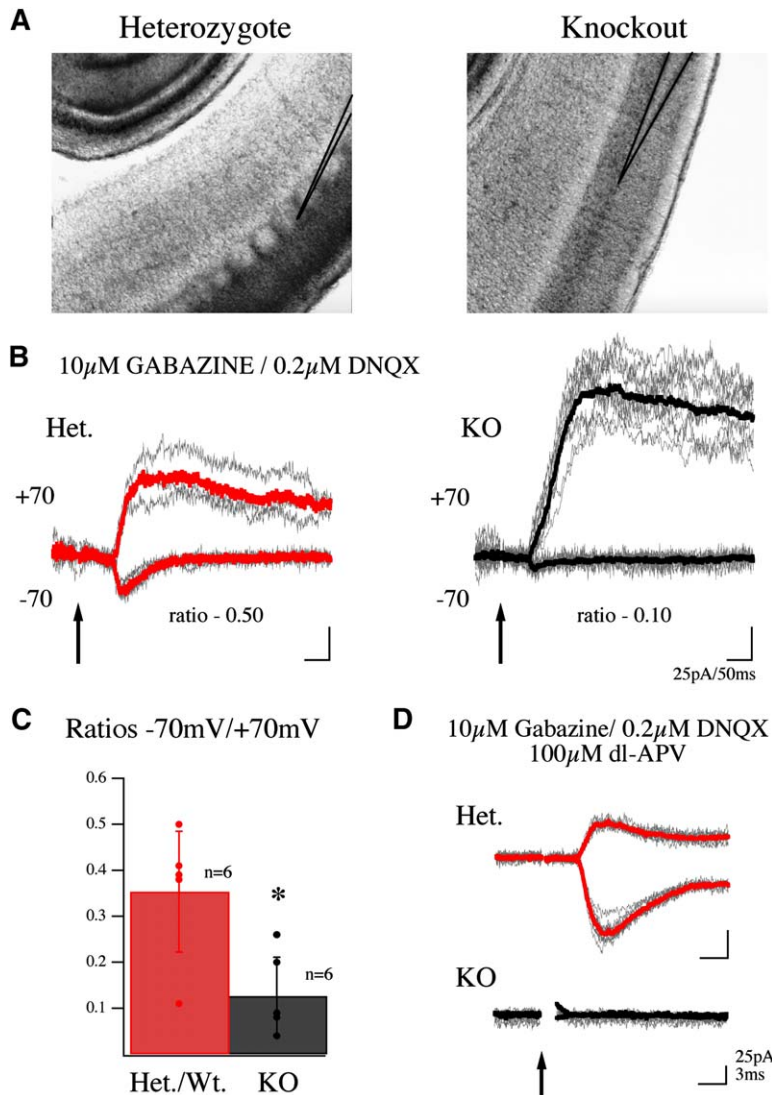
Figure 7. Altered Contribution of Ionotropic Glutamate Receptors to Synaptically Evoked Responses in Layer IV Cortical Neurons of *neuroD2* Null Mice

(A) DIC images of thalamocortical slices at 5× show the position of electrodes used to record from two of the neurons used in the analysis in part (B) and highlight the absence of barrel structures in layer IV of the knockout animals. Synaptic responses were evoked by white matter stimulation in both wild-type and knockout slices (stimulation at arrow) in the presence of a $GABA_A$ blocker and a low concentration of AMPAR antagonist (B and C). Whole-cell voltage-clamped responses in layer IV pyramidal neurons show postsynaptic currents evoked at a holding potential that isolates the AMPA-mediated current (-70 mV) due to the Mg^{2+}-dependent blockade of NMDARs and at a strongly depolarized potential ($+70$ mV) to reveal the complete postsynaptic current carried by ionotropic glutamate receptors (single traces are shown for each condition with overlaid average responses). In *neuroD2* null mice, a significant decrease was observed in the ratio of current recorded at -70 mV (20 ms poststimulation) in relation to the current at $+70$ mV (200 ms poststimulation) demonstrating an alteration in the relative contribution of NMDAR and AMPAR currents to the postsynaptic response at this synapse. (D) Addition of 100 μM dl-APV underscores this difference in receptor make-up by totally blocking the response at $+70$ mV in a knockout slice while revealing a fast AMPA-mediated response in a littermate heterozygous control slice (stimulation at arrow). Data are shown as mean ± SD.*$p < 0.05$ by t test.

due to the voltage-dependent magnesium block of NMDA receptors at this potential, while those evoked at +70 mV are mediated by all three receptors. The relative contribution of NMDA receptors to synaptic currents can therefore be gauged by recording synaptic responses at holding potentials of –70 and 70 mV. Analysis of responses in wild-type and neuroD2 null slices revealed that the mean ratio of peak responses at $-70/+70$ (AMPA + KA/AMPA + KA + NMDA) was significantly depressed in neuroD2 nulls compared to littermate controls (0.13 ± 0.08 versus 0.35 ± 0.13 mean ± SD) (Figures 7B and 7C). Addition of dl-APV (100 μM) totally blocked the current recorded at +70mV in the knockout slices but left a fast AMPA-mediated current in the wild-type slices, indicating that the knockout mice had very small AMPA currents (Figure 7D). This altered current ratio was also observed in the absence of pharmacological blockers when synaptic events were initiated through stimulation of the ventrobasal thalamus (Figure S6). Thus, the relative contribution of NMDA and non-NMDA receptors to synaptic responses is altered in *neuroD2* null mice, at least in part due to a reduction in AMPA receptor-mediated currents.

To further investigate the role of NeuroD2 in regulating the development of glutamatergic synapses, the NMDA antagonist dl-AP5 (100 μM) and the NMDA/AMPA antagonist GYKI-536555 (25 μM) were applied in sequence to determine the relative contributions of AMPA, NMDA, and KA receptors. The non-NMDA component includes contributions from AMPA and KA receptors. In both genotypes, approximately 20% of the response at –70 mV remained after blocking NMDA and AMPA receptors (with dl-APV and GYKI-536555), indicating that the relative KA contribution at this synapse was not significantly altered in *neuroD2* nulls (Figure 8A). By contrast, dl-APV alone resulted in a significantly higher fractional block in peak-current amplitude in knockout neurons compared to controls, indicating that non-NMDA receptors carry about 90% of the current in wild-type neurons, but only about 60% in *neuroD2* nulls (Figure 8A). These results further support the conclusion that the relative contribution of AMPA receptors is decreased and that of NMDA receptors is increased in *neuroD2* null mice. Consistent with this interpretation, the evoked response at 50 ms poststimulus in wild-type neurons at +70 mV was blocked to only 96% (±2.14%) by dl-AP5, while in
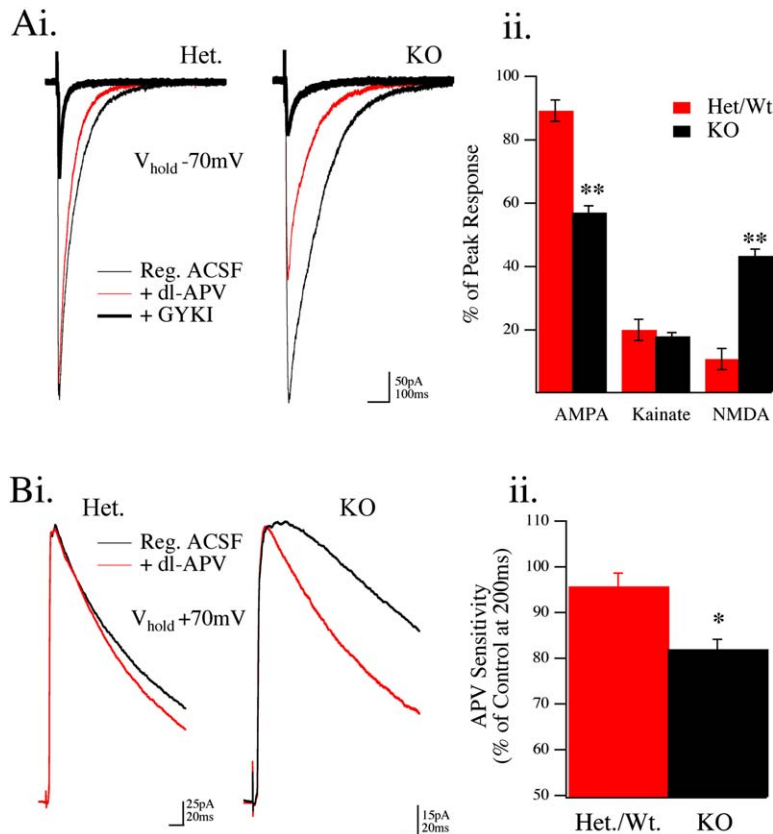
Figure 8. Pharmacology of Evoked Postsynaptic Responses in *neuroD2* Null Mice

The relative contribution of NMDAR current is increased in *neuroD2* null slices at P12. (Ai and Aii) Synaptic responses were evoked in layer IV neurons by white matter stimulation. Sequential application of the NMDA-specific antagonist dl-APV (100 μM) and the AMPA-specific antagonist GYKI 53655 (25 μM) was used to assess the contribution of different iGluRs at a holding potential of –70 mV. In wild-type/heterozygous slices, in the presence of 1.5 mM external Mg^{2+}, only 11% ± 5.0% (mean ± SE) of the peak postsynaptic current was carried by NMDARs. The contribution of NMDARs in ND2 null slices was significantly enhanced, as 43% ± 2.7% of the current was blocked by application of dl-APV (100 μM). The contribution of kainate receptors was unaltered (20% ± 3.3% versus 18% ± 1.2%, n = 5 wt/n = 3 ko) between wt/het and ko littermate control animals. (Bi and Bii) The contribution of NMDAR-mediated current was increased in the nulls when measured as the sensitivity to dl-APV at a holding potential of +70 mV, a voltage at which the Mg^{2+}-dependent block of this receptor is minimized. Under these conditions, dl-APV-sensitive current was significantly enhanced in neuroD2 null slices, when measured as a percent of pre-drug control response at 200 ms poststimulation (82 ± 2.1 versus 96 ± 2.9; mean ± SEM). Data are shown as mean ± SD. *p < 0.05 by t test.

neuroD2 null neurons the responses were blocked to 82% (±2.88%, mean ± SE, n = 4), indicating that a higher fraction of the synaptic current is carried by NMDA receptors in *neuroD2* null neurons (Figure 8B). Given previous evidence indicating that the relative contribution of AMPA receptors increases during development, these observations suggest that NeuroD2 is required for functional maturation of the postsynaptic response.

Altered Expression of Glutamate Receptor Subunits in *neuroD2* Null Mice
Our results demonstrating a reduced ratio of AMPA/NMDA synaptic responses in layer IV neurons in *neuroD2* knockout mice led us to investigate the distribution of glutamate receptors in barrel cortex. While we did not observe a consistent change in the distribution of NMDA receptors, immunofluorescence analysis with a GluR2/3 antibody indicated that there was a decrease in AMPA receptors in layer IV of barrel cortex in NeuroD2 null mice (Figures 9A–9I). We confirmed the specificity of the Glur2/3 antibody based on absence of staining in $gluR2^{-/-};gluR3^{-/-}$ double knockout brains (Figures 9J and 9K). To determine if surface expression of AMPA receptors was reduced in NeuroD2 null cortical neurons, we used surface labeling with GluR1 and GluR2 extracellular domain antibodies to visualize AMPA receptors in cortical cultures. As shown in Figure S7, surface labeling of both GluR1 and GluR2 was significantly reduced in neurons from *neuroD2* null mice. These observations suggest that NeuroD2 regulates synaptic maturation at least in part by regulating the expression and/or localization of AMPA receptors.

Discussion

The mechanisms that mediate activity-dependent development of cortical connections have been an area of active investigation for several decades. Initial studies focused on the role of synaptic receptors in this process and revealed a key role for calcium influx via NMDA receptors (Iwasato et al., 2000; Sawtell et al., 2003; reviewed in Bear and Rittenhouse, 1999). Our interest in transcriptional mediators of calcium signaling motivated us to carry out a screen for calcium-activated transcription factors and led to the cloning of NeuroD2. Here we show that NeuroD2 plays a critical role in regulating both the anatomical and physiological maturation of thalamocortical connections (Figure 10).

While we have not yet determined the mechanisms of NeuroD2 activation by calcium signaling, preliminary experiments suggest that it may be regulated by CaM kinase IV signaling. A constitutively active form of CaM kinase IV is sufficient to induce NeuroD2-mediated transcription, and overexpression of wild-type CaM kinase IV enhances calcium-dependent activation of NeuroD2 (G.I-D. and A.G, unpublished data). NeuroD, which is related to NeuroD2, was recently shown to be calcium regulated and requires phosphorylation of a key serine residue for activation (Gaudilliere et al., 2004). This serine is conserved in NeuroD2 (Ser336) and represents a potential site of regulation for NeuroD2. The fact that both NeuroD and NeuroD2 act as calcium-regulated transcription factors identifies this protein family as a major target of calcium signaling in neurons.
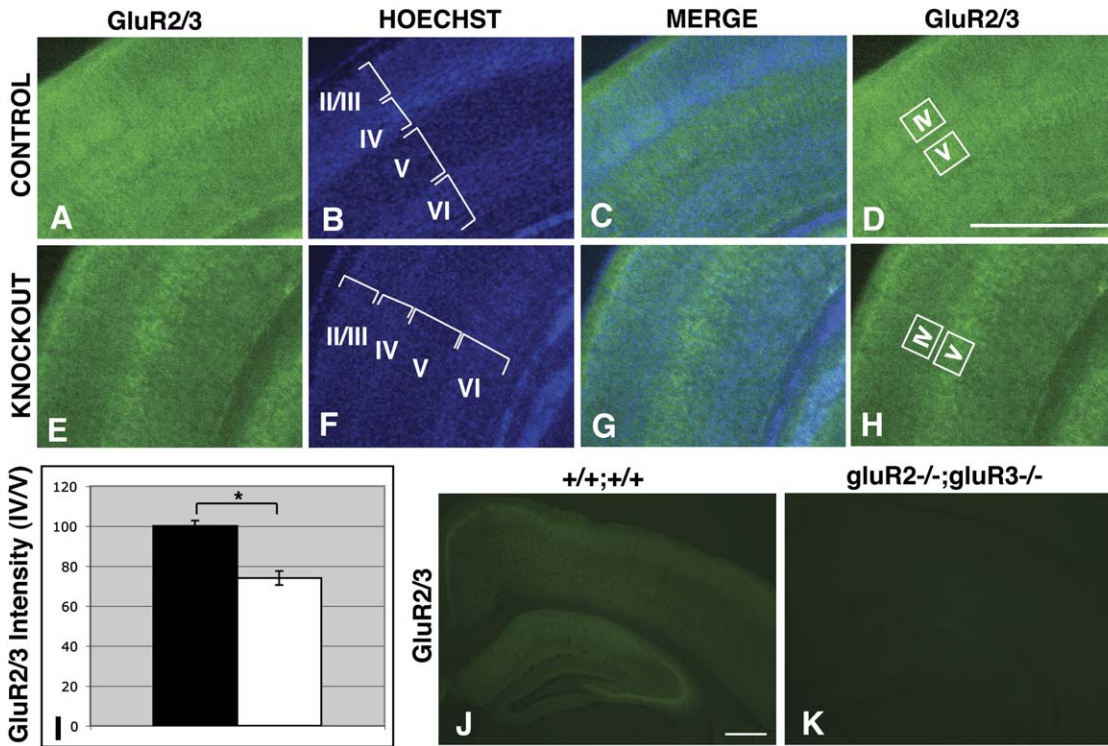
Figure 9. Reduction in AMPA Receptor Distribution in Layer IV of *neuroD2* Null Mice

(A and E) Coronal sections from control and neuroD2 knockout mice at age P7 immunostained using an antibody recognizing the GluR2 and GluR3 subunits of the AMPA receptor. Staining is present in all layers and in a barrel-specific pattern in layer IV. Layer IV-specific immunostaining is reduced in knockouts.

(B and F) Layers II–VI are marked on sections stained with nuclear dye Hoechst 33258.

(C and G) Merged images of GluR2/3 immunoflouresence and Hoechst 33258 nuclear dye.

(D and H) Regions of interest in layers IV and V used to measure the relative abundance of GluR2/3 in layer IV in wild-type and *neuroD2* null mice.

(I) Ratio of GluR2/3 signal intensity in layer IV/layer V in control (blackbar) and *neuroD2* null (whitebar) mice.

(J and K) Sections from $gluR2^{-/-};gluR3^{-/-}$ double knockout and wild-type control mice stained with an antibody recognizing GluR2 and GluR3 subunits. Staining is completely absent in the double knockout mouse, demonstrating antibody specificity.

Data shown are representative examples based on analysis of several sections from two wild-type/knockout pairs and are presented as mean ± SEM. Asterisks indicate $p < 0.05$ by t test. Scale bars, 500 μm.

Our case for a critical role for NeuroD2 in thalamocortical patterning is based on analysis of mice carrying a targeted mutation in the *neuroD2* gene. These mice are born in normal Mendelian ratio, but most die between 4 to 5 weeks of age. Both *neuroD2* null and heterozygous mice show differences in brain organization
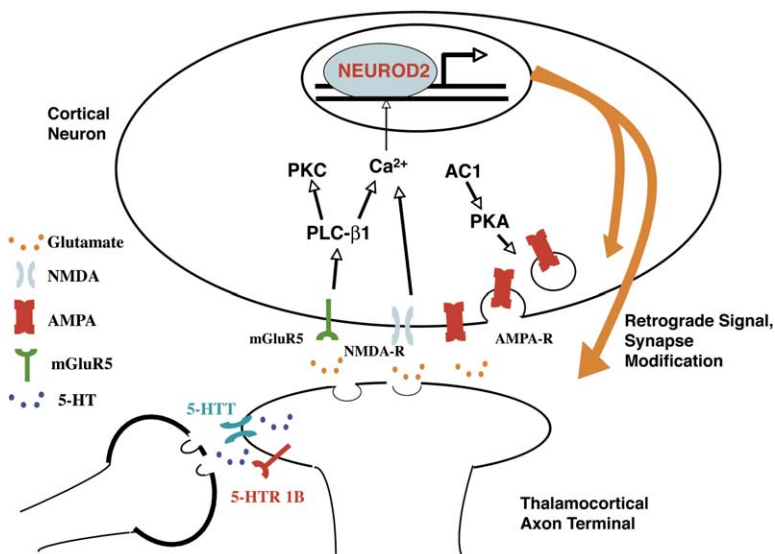
Figure 10. Diagrammatic Representation of the Proposed Role of NeuroD2 in the Development of Thalamocortical Connections

Calcium influx regulates NeuroD2-mediated gene expression in cortical neurons. These gene products influence both the development of thalamocortical axon terminals and the maturation of the thalamocortical synapse.

compared to wild-type littermates, including a decrease in brain size, a slightly smaller and rounder hippocampus, and absence of corpus callosum. These differences per se appear not to be responsible for the barrel cortex defects seen in *neuroD2* null mice, since these anatomical differences are present in both knockout and heterozygous mice, but heterozygous mice do not display any defects in barrel cortex. Also, several other mutant mice with cortical development defects, including smaller brains, absence of corpus callosum, lamination defects, and poorly developed dendrites, have no defects with respect to organization of barrel units (Land and Monaghan, 2003; Aizawa et al., 2004). For example, *crest* mutant mice, which we previously reported as having defects in dendrite development, do not have any defect in barrel cortex (Aizawa et al., 2004; H. Aizawa and A.G., unpublished data). Thus, perturbation of barrel cortex patterning is not a nonspecific consequence of a brain development defect. Instead our observations argue that the barrel cortex defect in *neuroD2* null mice is a result of a specific absence of cortical NeuroD2 function.

How might NeuroD2 contribute to patterning of the thalamocortical projections? We propose that NeuroD2 regulates the expression of factors that are required for both the anatomical development and synaptic maturation of thalamocortical connections. With regard to the patterning of thalamocortical axons, it is relevant that NeuroD2 binds to the GAP-43 promoter, since GAP-43 mutant mice have a defect in barrel formation, and the specific defects are strikingly similar to those seen in *neuroD2* mutants (Maier et al., 1999). Interestingly, we find that GAP-43 levels are reduced in barrel cortex in *neuroD2* null mice at P3 and P7, as well as in cultured cortical neurons isolated from the knockouts (Figure S5). Although GAP-43 is generally considered a predominantly axonal protein, we can detect GAP-43 in dendrites in cortical cultures using a phospho-GAP-43 antibody (Figure S5). This raises the possibility that NeuroD2 might regulate levels of GAP-43 in layer IV neurons. While we cannot conclude that the failure of thalamocortical axon segregation in *neuroD2* nulls is due to an effect on GAP-43 expression, the relationship between *neuroD2* and GAP-43 as well as the mutant phenotypes suggests that loss of GAP-43 in *neuroD2* nulls probably contributes to the observed phenotype.

The effects of loss of NeuroD2 on the functional development of thalamocortical synapses are striking and suggest that NeuroD2 may generally be involved in regulating glutamatergic synapse maturation. The relative contribution of AMPA, KA, and NMDA receptor-mediated excitatory responses is tightly regulated during the first week of development in the barrel cortex. Early on (P3–P5), many thalamocortical synapses are composed of mostly NMDA receptor currents and are termed "silent synapses" due to their lack of response to stimulation at resting membrane potentials (Isaac et al., 1997). By the end of the first postnatal week, the contribution of NMDA receptor responses decreases and the AMPA component increases. The switch in relative contribution of NMDA and AMPA receptors at the thalamocortical synapse coincides with a loss of ability to induce LTP and LTD (Crair and Malenka, 1995; Feldman et al., 1998). It is hypothesized that an NMDA receptor-dependent LTP-like mechanism induces the incorporation of functional AMPA receptors into silent synapses, hence unmasking them. In *neuroD2* null mice, the relative NMDA component of postsynaptic EPSCs are significantly higher and AMPA are lower than responses of wild-type littermates, suggesting that NeuroD2 is involved in the mechanism by which NMDA receptor activation leads to a maturation of the AMPA current.

Mechanistic insight into the role of NeuroD2 in regulating the maturation of synaptic responses comes from the expression of glutamate receptor subunits in *neuroD2* null mice. While the overall levels of NMDA and AMPA receptors in the cortex are not significantly affected in *neuroD2* nulls, the expression in layer IV is notably affected. In wild-type mice, the expression of GluR2/3 subunits is prominent in barrels in layer IV. This pattern is completely missing in *neuroD2* nulls, and the levels of receptor expression in layer IV compared to adjacent layers are reduced in *neuroD2* nulls. Thus, one possibility is that NeuroD2 regulates expression of glutamate receptors in layer IV and that loss of that regulation leads to failure of synaptic maturation. It is also noteworthy that several genes involved in receptor and vesicle trafficking are altered in *neuroD2* mutant mice (Olson et al., 2001), suggesting that NeuroD2 may be involved in proper targeting of NMDA or AMPA receptors. Consistent with a potential role for NeuroD2 in receptor trafficking, we observe a significant decrease in surface expression of GluR1 and GluR2 in cultured cortical neurons isolated from *neuroD2* null mice compared to controls.

In summary, our observations identify NeuroD2 as a key transcriptional mediator of thalamocortical patterning. We find that NeuroD2-mediated transcription is calcium regulated and that loss of NeuroD2 leads to a failure in thalamocortical axon segregation and to a disruption in glutamatergic synapse maturation. By regulating both the anatomical and physiological development of thalamocortical connections, NeuroD2 appears to play a central role in the establishment and maturation of cortical connections.

Experimental Procedures

Primary Cell Cultures and Transactivation Assays

The isolation of *neuroD2* using the transactivator trap screen was performed as described previously (Aizawa et al., 2004). E18 cortical neurons from Long-Evans rat embryos were cultured in Basal Medium Eagle supplemented with L-glutamine, antibiotics, fetal bovine serum and N2-supplement for 3 days and then transfected with the desired constructs using the calcium-phosphate method (Threadgill et al., 1997). At 4DIV, neurons were stimulated with 50 mM KCl for 16 hr and were fixed with 4% paraformaldehyde (PFA) and 4% sucrose in phosphate-buffered saline (PBS). Activation of the CAT reporter gene was assessed by either immunohistochemistry using the anti-CAT antibody (Sigma) or chloramphenicol acetyl transferase (CAT) assay, as described previously (Shieh et al., 1998). Luciferase assays were performed using the Dual Luciferase Assay Kit (Promega), as recommended in the producer's manual.

Plasmids

The following plasmids have been described previously: rat brain cDNA library used in the transactivator trap screen (Aizawa et al., 2004), UAS-CAT (Martin et al., 1990), Gap43-luciferase (McCormick et al., 1996). To generate the Gal4DBD-NeuroD2 constructs, full-length and deletion fragments of mouse *neuroD2* cDNA were

amplified from pCS2-mND2 (McCormick et al., 1996), using Pfx DNA polymerase and subcloned into the expression vector pRK5, which includes a Gal4DBD insert. All constructs generated were validated by direct sequencing.

Mouse Colony Management

Heterozygous (lacZ/+) mice maintained in the 129SvJ background were used as breeding pairs. (lacZ/+) or (+/+) littermates were used as controls in all experiments. *neuroD2* null mice were lacZ/lacZ.

Histology and Immunostaining

Control and *neuroD2* pups were perfused at the indicated ages with freshly prepared 4% PFA in PBS. The brains were postfixed in 4% PFA overnight at 4°C and then cryoprotected in PBS containing 30% sucrose. The brains were sectioned in the desired plane using a freezing cryostat for immunostaining, β-galactosidase (β-Gal) assays, CO staining, and cresyl violet staining. For CO staining, sections were incubated in 25 mg DAB, 15 mg cytochrome C, 1 g sucrose in 50 ml 0.1 M phosphate buffer (pH 7.4) in a 37°C shaker. For immunofluorescence, sections were blocked with 3% Bovine-Serum Albumin (BSA), 0.3% Triton X-100 in PBS for 2 hr. NeuN (Chemicon), S100-β (Sigma), GluR2/3 (rabbit polyclonal) antibodies were added at 1:200–1:1000 concentration to blocking solution and incubated overnight. Alexa Fluor 488 conjugated anti-mouse immunoglobulins (Molecular Probes) were used as secondary antibodies. For 5-HT immunohistochemistry, sections were blocked in 5% nonfat dry milk powder, 0.3% Triton X-100, and 10% Normal Goat Serum in PBS for 2 hr, and 5-HT antibody (Diasorin) was added to 1:10000 dilution to the blocking solution and incubated for 48 hr. Biotinylated anti-rabbit secondary antibody incubation was followed by DAB staining. For β-Gal assays, sections were incubated overnight in 0.5 mg/ml X-gal in LacZ stain solution (Lober et al., 1999). Sections were stained in 5 mg/ml cresyl violet dye. Hoechst 33258 DNA dye was used at 1.25 μg/ml final concentration. Images were captured by Zeiss Axioscope microscope using the OpenLab software. Experiments were analyzed blind to genotype.

For live-labeling experiments, 21DIV cultured neurons from wild-type and knockout animals were live-labeled with either rabbit anti-GluR1 (Calbiochem; 1:10) or mouse anti-GluR2 (Chemicon; 1:100) antibodies for 15 min in Opti-Mem (Gibco) and 0.1% sodium azide, rinsed 3 × 5 min in PBS, then fixed for 15 min in 4% PFA, 4% sucrose. Neurons were blocked with 3% BSA, 0.15% Triton X-100 in PBS for 30 min, then stained with chicken anti-MAP2 antibody (Abcam; 1:5000) for 1 hr. Alexa 488 anti-mouse or rabbit (Molecular Probes; 1:1000) and Cy3 anti-chicken (Jackson Laboratories; 1:1000) were used as secondary antibodies. Images were captured on a Leica confocal microscope using a 63× oil-immersion objective and then analyzed using OpenLab software.

DiI and DiA Labeling

Littermate mice were perfused as described above and postfixed in 4% PFA overnight. DiI and DiA crystals were injected into the cortical plates at two distinct locations within the barrel cortex for retrograde TCA labeling. DiI crystals were injected into the dorsal thalamus for anterograde TCA labeling. Brains were incubated in PBS in dark at 37°C for 4–5 weeks, sectioned in the coronal plane to 100–300 μm slices using a vibratome, and counterstained with Hoechst 33258. Images of DiI- and DiA-labeled thalamic cell bodies or cortical barrels were captured using confocal microscopy (Zeiss Axiovert 200 microscope, PerkinElmer UltraView System).

Immunoblotting

Littermate mice were anesthetized, rapidly decapitated, and their cortices were dissected in ice-cold PBS. Individual cortices were homogenized in Lysis Buffer (25 mM Tris, pH 7.5, 50 mM NaCl, 5 mM EGTA, 5 mM EGTA) by sonication. Protein concentrations were quantified by Bradford Method. Equal amounts of protein were run in SDS-PAGE system for Western blotting. The following antibodies were used: GluR1, GluR3, NR1, NR2A, NR2B (generous gift of Rick Huganir), GluR2 (Zymed Lab. Inc.), and GAP-43 (Zymed Lab. Inc.). Immunoblots were simultaneously probed with anti-actin or tubulin antibody (Sigma) as loading control. Individual bands were quantified using Quantity One software (Bio-Rad Laboratories).

Electrophysiology

Mice (P11–P13) were anesthetized using halothane (2-bromo-2-chloro-1,1,1-trifluoroethane, Sigma Chemical) and rapidly decapitated. Brains were quickly removed and immersed in oxygenated (95% O_2/5% CO_2), ice-cold, bicarbonate-buffered, sucrose-substituted saline containing (in mM): 212 sucrose, 26 $NaHCO_3$, 1.23 NaH_2PO_4, 2.6 KCl, 3 $MgCl_2$, 1 $CaCl_2$, and 10 glucose. Coronal slices or thalamocortical slices (400 μm thick) were cut on a vibrating tissue slicer (Series 1000/1500, Vibratome) and placed in an oxygenated recording solution containing (in mM): 124 NaCl, 5 KCl, 26 $NaHCO_3$, 1.23 NaH_2PO_4, 1.5 $MgCl_2$, 2 $CaCl_2$ and 10 glucose. Slices were left to equilibrate at 35°C or at room temperature for at least 1 hr. Drugs: dl-AP5, gabazine (SR 95531 hydrobromide), and DNQX were acquired from Tocris Chemicals (MO) and mixed according to manufacturer's specifications. GYKI 53655 was a generous gift from Gyula Horvath at IVAX pharmaceuticals (Budapest, Hungary).

Voltage-clamp recordings were made using glass microelectrodes (filamented borosilicate glass 1.5 mm O.D. and 0.86 mm I.D., Harvard Instruments) pulled on a micropipette puller (Flaming-Brown P-80/PC, Sutter Instruments Co.), and filled with a cesium-substituted intracellular solution containing 10 mM CsCl, 105 mM $CsMeSO_3$, 8 mM NaCl, 0.5 mM ATP, 0.3 mM GTP, 10 mM HEPES, 5 mM glucose, 2 mM $MgCl_2$, 1 mM EGTA, 5 mM TEA, 1 mM QX314, pH 7.3. This intracellular solution also included 10 mM BAPTA to avoid potentiation during repeated steps to +70 mV. The junction potential was 10–13 mV and is not corrected for in the values presented. Input impedance measurements were not significantly different between wild-type and neuroD2 null neurons under these conditions.

The standard recording solution used for current-clamp measurements contained 120 mM KGluconate in lieu of the Cs salts and lacked TEA, QX314, and BAPTA. Under these conditions, the effective input impedance ranged from 381 to 481 MΩ in knockout cells and 612 to 634 MΩ in wild-type neurons. This difference in input impedance may be related to differences in dendritic length in wild-type and *neuroD2* null animals (G.I.-D. and A.G., unpublished data). Intracellular solutions were typically matched to extracellular osmolarity. Pipette resistances ranged from 2 to 8 MΩ. Series resistance ranged from ≈7 to 25 MΩ and was monitored for consistency during recording. Stimulation electrodes were concentric bipolar (Frederick Haer & Co.) with a 200 μm stainless-steel outer pole and a 25 μm diameter inner pole of platinum iridium. Electrical stimulation was accomplished via a stimulus-isolation unit (S.I.U. 90, Neuro Data Inst. Corp.) driven by a digital stimulator (PG4000, Neuro Data). Signals were recorded using patch-clamp amplifiers (PC505B, Warner Inst. Corp.) and digitized with a PCI-based board (PCI-1200, National Instruments) on a Macintosh G3 computer using custom-written software in Igor Pro (Wavemetrics). Signals were amplified, sampled at 10 kHz, filtered to 1 or 2 kHz, and analyzed using custom routines in Igor Pro. Recordings made under $GABA_A$ block to remove Cl^- current contamination (10 or 20 μM gabazine) also included a low concentration of DNQX (0.2 μM) to avoid epileptiform-like activity and synaptic overexcitation.

References

Abdel-Majid, R.M., Leong, W.L., Schalkwyk, L.C., Smallman, D.S., Wong, S.T., Storm, D.R., Fine, A., Dobson, M.J., Guernsey, D.L., and Neumann, P.E. (1998). Loss of adenylyl cyclase I activity disrupts patterning of mouse somatosensory cortex. Nat. Genet. *19*, 289–291.

Agmon, A., and Connors, B.W. (1992). Correlation between intrinsic firing patterns and thalamocortical synaptic responses of neurons in mouse barrel cortex. J. Neurosci. *12*, 319–329.

Agmon, A., Yang, L.T., O'Dowd, D.K., and Jones, E.G. (1993). Organized growth of thalamocortical axons from the deep tier of terminations into layer IV of developing mouse barrel cortex. J. Neurosci. *13*, 5365–5382.

Aizawa, H., Hu, S.C., Bobb, K., Balakrishnan, K., Ince, G., Gurevich, I., Cowan, M., and Ghosh, A. (2004). Dendrite development regulated by CREST, a calcium-regulated transcriptional activator. Science *303*, 197–202.

Bear, M.F., and Rittenhouse, C.D. (1999). Molecular basis for induction of ocular dominance plasticity. J. Neurobiol. *41*, 83–91.

Crair, M.C. (1999). Neuronal activity during development: permissive or instructive? Curr. Opin. Neurobiol. *9*, 88–93.

Crair, M.C., and Malenka, R.C. (1995). A critical period for long-term potentiation at thalamocortical synapse. Nature *375*, 325–328.

Erzurumlu, R.S., and Kind, P.C. (2001). Neural activity: sculptor of 'barrels' in the neocortex. Trends Neurosci. *24*, 589–595.

Feldman, D.E., Nicoll, R.A., Malenka, R.C., and Isaac, J.T. (1998). Long-term depression at thalamocortical synapse in developing rat somatosensory cortex. Neuron *21*, 347–357.

Fox, K. (2002). Anatomical pathways and molecular mechanisms for plasticity in the barrel cortex. Neuroscience *111*, 799–814.

Gaudilliere, B., Konishi, Y., de la Iglesia, N., Yao, G., and Bonni, A. (2004). A CaMKII-NeuroD signaling pathway specifies dendritic morphogenesis. Neuron *41*, 229–241.

Ghosh, A., and Greenberg, M.E. (1995). Calcium signaling in neurons: molecular mechanisms and cellular consequences. Science *268*, 239–247.

Hannan, A.J., Blakemore, C., Katsnelson, A., Vitalis, T., Huber, K.M., Bear, M., Roder, J., Kim, D., Shin, H.S., and Kind, P.C. (2001). PLC-beta1, activated via mGluRs, mediates activity-dependent differentiation in cerebral cortex. Nat. Neurosci. *4*, 282–288.

Isaac, J.T., Crair, M.C., Nicoll, R.A., and Malenka, R.C. (1997). Silent synapses during development of thalamocortical inputs. Neuron *18*, 269–280.

Iwasato, T., Datwani, A., Wolf, A.M., Nishiyama, H., Taguchi, Y., Tonegawa, S., Knopfel, T., Erzurumlu, R.S., and Itohara, S. (2000). Cortex-restricted disruption of NMDAR1 impairs neuronal patterns in the barrel cortex. Nature *406*, 726–731.

Katz, L.C., and Shatz, C.J. (1996). Synaptic activity and the construction of cortical circuits. Science *274*, 1133–1138.

Land, P.W., and Monaghan, A.P. (2003). Expression of the transcription factor, tailless, is required for formation of superficial cortical layers. Cereb. Cortex *13*, 921–931.

Lebrand, C., Cases, O., Adelbrecht, C., Doye, A., Alvarez, C., El Mestikawy, S., Seif, I., and Gaspar, P. (1996). Transient uptake and storage of serotonin in developing thalamic neurons. Neuron *17*, 823–835.

Lein, E.S., and Shatz, C.J. (2000). Rapid regulation of brain-derived neurotrophic factor mRNA within eye-specific circuits during ocular dominance column formation. J. Neurosci. *20*, 1470–1483.

Lin, C.H., Stoeck, J., Ravanpay, A.C., Guillemot, F., Tapscott, S.J., and Olson, J.M. (2004). Regulation of neuroD2 expression in mouse brain. Dev. Biol. *265*, 234–245.

Lober, S., Hubner, H., and Gmeiner, P. (1999). Azaindole derivatives with high affinity for the dopamine D4 receptor: synthesis, ligand binding studies and comparison of molecular electrostatic potential maps. Bioorg. Med. Chem. Lett. *9*, 97–102.

Lu, H.C., Gonzalez, E., and Crair, M.C. (2001). Barrel cortex critical period plasticity is independent of changes in NMDA receptor subunit composition. Neuron *32*, 619–634.

Lu, H.C., She, W.C., Plas, D.T., Neumann, P.E., Janz, R., and Crair, M.C. (2003). Adenylyl cyclase I regulates AMPA receptor trafficking during mouse cortical 'barrel' map development. Nat. Neurosci. *6*, 939–943.

Maier, D.L., Mani, S., Donovan, S.L., Soppet, D., Tessarollo, L., McCasland, J.S., and Meiri, K.F. (1999). Disrupted cortical map and absence of cortical barrels in growth-associated protein (GAP)-43 knockout mice. Proc. Natl. Acad. Sci. USA *96*, 9397–9402.

Martin, K.J., Lillie, J.W., and Green, M.R. (1990). Evidence for interaction of different eukaryotic transcriptional activators with distinct cellular targets. Nature *346*, 147–152.

McCormick, M.B., Tamimi, R.M., Snider, L., Asakura, A., Bergstrom, D., and Tapscott, S.J. (1996). NeuroD2 and NeuroD3: distinct expression patterns and transcriptional activation potentials within the neuroD gene family. Mol. Cell. Biol. *16*, 5792–5800.

Olson, J.M., Asakura, A., Snider, L., Hawkes, R., Strand, A., Stoeck, J., Hallahan, A., Pritchard, J., and Tapscott, S.J. (2001). NeuroD2 is necessary for development and survival of central nervous system neurons. Dev. Biol. *234*, 174–187.

Pham, T.A., Impey, S., Storm, D.R., and Stryker, M.P. (1999). CRE-mediated gene transcription in neocortical neuronal plasticity during the developmental critical period. Neuron *22*, 63–72.

Qiu, M., Anderson, S., Chen, S., Meneses, J.J., Hevner, R., Kuwana, E., Pedersen, R.A., and Rubenstein, J.L. (1996). Mutation of the Emx-1 homeobox gene disrupts the corpus callosum. Dev. Biol. *178*, 174–178.

Rosen, K.M., McCormack, M.A., Villa-Komaroff, L., and Mower, G.D. (1992). Brief visual experience induces immediate early gene expression in the cat visual cortex. Proc. Natl. Acad. Sci. USA *89*, 5437–5441.

Sawtell, N.B., Frenkel, M.Y., Philpot, B.D., Nakazawa, K., Tonegawa, S., and Bear, M.F. (2003). NMDA receptor-dependent ocular dominance plasticity in adult visual cortex. Neuron *38*, 977–985.

Senft, W.L., and Woolsey, T.A. (1991). Growth of thalamic afferents into mouse barrel cortex. Cereb. Cortex *1*, 308–335.

Shen, Y., Mani, S., Donovan, S.L., Schwob, J.E., and Meiri, K.F. (2002). Growth-associated protein-43 is required for commissural axon guidance in the developing vertebrate nervous system. J. Neurosci. *22*, 239–247.

Shieh, P.B., Hu, S.C., Bobb, K., Timmusk, T., and Ghosh, A. (1998). Identification of a signaling pathway involved in calcium regulation of BDNF expression. Neuron *20*, 727–740.

Threadgill, R., Bobb, K., and Ghosh, A. (1997). Regulation of dendritic growth and remodeling by Rho, Rac, and Cdc42. Neuron *19*, 625–634.

Wallace, M.N. (1987). Histochemical demonstration of sensory maps in the rat and mouse cerebral cortex. Brain Res. *418*, 178–182.

Welker, C. (1976). Receptive fields of barrels in the somatosensory neocortex of the rat. J. Comp. Neurol. *166*, 173–189.

West, A.E., Chen, W.G., Dalva, M.B., Dolmetsch, R.E., Kornhauser, J.M., Shaywitz, A.J., Takasu, M.A., Tao, X., and Greenberg, M.E. (2001). Calcium regulation of neuronal gene expression. Proc. Natl. Acad. Sci. USA *98*, 11024–11031.

Woolsey, T.A., and Van der Loos, H. (1970). The structural organization of layer IV in the somatosensory region (SI) of mouse cerebral cortex. The description of a cortical field composed of discrete cytoarchitechtonic units. Brain Res. *17*, 205–242.